Thioester hydrolysis reactivity of zinc hydroxide complexes: investigating reactivity relevant to glyoxalase II enzymes†

Lisa M. Berreau,*[a] Amrita Saha[a] and Atta M. Arif[b]

Received 5th September 2005, Accepted 17th October 2005
First published as an Advance Article on the web 23rd November 2005
DOI: 10.1039/b512515d

A recently reported binuclear zinc hydroxide complex $[(L^1Zn_2)(\mu\text{-}OH)](ClO_4)_2$ (**1**, L^1 = 2,6-bis[(bis(2-pyridylmethyl)amino)methyl]-4-methylphenolate monoanion) containing a single bridging hydroxide was examined for thioester hydrolysis reactivity. Treatment of **1** with hydroxyphenylthioacetic acid *S*-methyl ester in dry CD_3CN results in no reaction after ~65 h at 45(1) °C. Binuclear zinc hydroxide complexes of the *N*-methyl-*N*-((6-neopentylamino-2-pyridyl)methyl)-*N*-((2-pyridyl)methyl)amine (L^2) and *N*-methyl-*N*-((6-neopentylamino-2-pyridyl)methyl)-*N*-((2-pyridyl)ethyl)amine (L^3) chelate ligands were prepared by treatment of each ligand with molar equivalent amounts of $Zn(ClO_4)_2\cdot 6H_2O$ and KOH in methanol. These complexes, $[(L^2Zn)_2(\mu\text{-}OH)_2](ClO_4)_2$ (**2**) and $[(L^3Zn)_2(\mu\text{-}OH)_2](ClO_4)_2$ (**3**), which have been structurally characterized by X-ray crystallography, behave as 1 : 1 electrolytes in acetonitrile, indicating that the binuclear cations dissociate into monomeric zinc hydroxide species in solution. Treatment of **2** or **3** with one equivalent of hydroxyphenylthioacetic acid *S*-methyl ester per zinc center in acetonitrile results in the formation of a zinc α-hydroxycarboxylate complex, $[(L^2)Zn(O_2CCH(OH)Ph)]ClO_4\cdot 1.5H_2O$ (**4**) or $[(L^3)Zn(O_2CCH(OH)Ph)]ClO_4\cdot 1.5H_2O$ (**5**), and CH_3SH. These reactions, to our knowledge, are the first reported examples of thioester hydrolysis mediated by zinc hydroxide complexes. The results of this study suggest that a terminal Zn–OH moiety may be required for hydrolysis reactivity with a thioester substrate.

Introduction

The glyoxalase system, which is comprised of two metalloenzymes, glyoxalase I (GLX1) and glyoxalase II (GLX2) and is found in several organisms including humans, catalyzes the conversion of 2-oxoaldehydes to 2-hydroxycarboxylic acids.[1] An important substrate for this system is methyl glyoxal, $CH_3C(O)CHO$, a reactive small molecule that is produced as a byproduct of lipid and carbohydrate metabolism.[2,3] Methyl glyoxal is toxic and mutagenic due to the reactivity of the aldehyde group with guanine residues of DNA and amino acid nucleophiles, such as the amino groups of arginine and lysine, and the thiolate moiety of cysteine.[4,5] As shown in Scheme 1, GLX1 catalyzes the isomerization of a hemithioacetal to yield a 2-hydroxythioester. GLX2 catalyzes the hydrolysis of this thioester to produce a 2-hydroxy acid (*e.g.* lactic acid) and free glutathione.

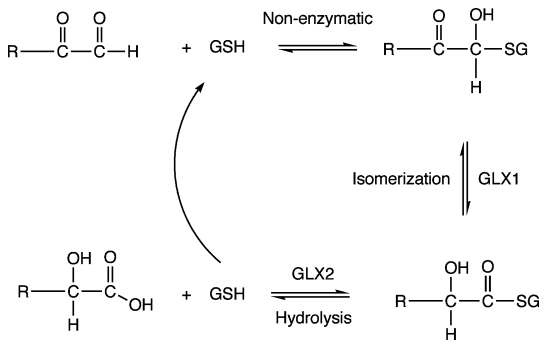

Scheme 1 Reactions catalyzed by GLX1 and GLX2. GSH is reduced glutathione.

Crystal structures of human GLX2 derived from two different crystallization conditions have been reported.[6] Based on sequence homology, GLX2 has been identified as a member of the metallo-β-lactamase superfamily of hydrolases[7,8] and contains a binuclear metal cluster within the active site. Metal analysis of the protein used for X-ray crystallographic studies indicated the presence of ~1.5 moles of zinc and ~0.7 moles of iron per protein. Despite this variable metal ion content, the structure of human GLX2 was described as having a binuclear zinc active site cluster, a description that was based in part on comparison of human GLX2 to the analogous enzyme isolated from *A. thaliana*, which was initially described as a zinc enzyme.[6,9] Overall, the results of the crystallographic studies indicate that the two metal centers in GLX2 are separated by ~3.3–3.5 Å, depending on crystallization conditions, and are bridged by a water/hydroxo moiety and a single oxygen atom from Asp134 (Fig. 1). The remaining zinc ligands are nitrogen atom donors from histidine ligands, and one monodentate aspartate donor coordinated to the M_2 ion.

[a]*Department of Chemistry and Biochemistry, Utah State University, 0300 Old Main Hill, Logan, UT, 84322-0300, USA. E-mail: berreau@cc.usu.edu; Fax: +1 435-797-3390; Tel: +1 435-797-1625*
[b]*Department of Chemistry, University of Utah, 315 S. 1400 E., Salt Lake City, UT, 84112-0850, USA. E-mail: arif@chemistry.utah.edu*

† Electronic supplementary information (ESI) available: Preparation of **1**. Table S1: Crystallographic data for $\mathbf{1}\cdot 3CH_3CN$. Table 2: Selected bond lengths and angles for $\mathbf{1}\cdot 3CH_3CN$. Fig. S1: Cationic portion of the X-ray structure of $\mathbf{1}\cdot 3CH_3CN$. Fig. S2: Space-filling model of the cationic portion of $\mathbf{1}\cdot 3CH_3CN$. Fig. S3: ^1H NMR spectra of analytically pure **2** and **3** in dry CD_3CN. See DOI: 10.1039/b512515d

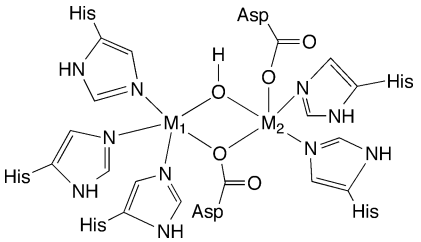

Fig. 1 Structural features of the binuclear metal cluster in the active site of human GLX2. The description of the X-ray structure has M_1/M_2 = Zn(II).[6]

The metal coordination environment in human GLX2 is influenced by the presence of anions and substrate/inhibitor-type molecules. For example, a crystallographic data set collected on human GLX2 crystals grown from a solution containing acetate and cacodylate ($(CH_3)_2AsO_2^-$) ions revealed an asymmetric unit comprised of two binuclear metal sites, both of which contain a coordinated bridging μ-1,2-$O_2As(CH_3)_2$ anion. In this case, the metal centers each exhibit an overall coordination number of six and a distorted octahedral geometry. A second crystallographic data set, obtained from crystals soaked in a solution containing the slow substrate *S*-(*N*-hydroxy-*N*-bromophenylcarbamoyl)glutathione (HBPC-GSH), revealed a HBPC-GSH substrate molecule bound near one binuclear metal site of the asymmetric unit, whereas the product GSH ($M_2 \cdots$ S(thiol) ~2.9 Å) was found located near the other binuclear metal site. In the HBPC-GSH bound site of the asymmetric unit, the thioester carbonyl oxygen is positioned near M_1 ($M_1 \cdots$ O(thioester) ~3.3 Å) and the HBPC-GSH sulfur atom is ~3.3 Å from M_2. In this structural arrangement, the bridging water/hydroxo moiety is ~2.9 Å from the carbonyl carbon of the thioester substrate. The α-hydroxyl group of HBPC-GSH does not interact with the binuclear metal center or *via* hydrogen bonding with the protein.

Based on these X-ray crystallographic studies, a mechanism for thioester hydrolysis by zinc-containing human GLX2 has been proposed (Scheme 2).[6] This pathway involves attack of the bridging hydroxide moiety on the thioester carbonyl group, with the Zn_1 center being involved in stabilization of the transition state. It has also been suggested that Zn_2 may stabilize the glutathione thiolate moiety formed upon C–S bond cleavage.

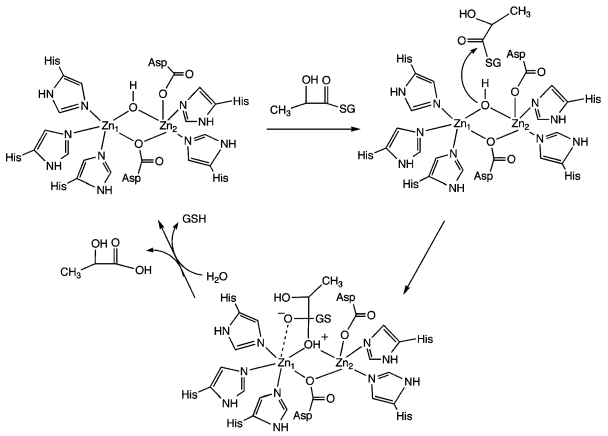

Scheme 2 Proposed mechanism for zinc-containing human GLX2.[6]

In the past few years, extensive studies have been performed on the cytoplasmic GLX2 enzyme obtained from *Arabidopsis thaliana*, which has more than 50% sequence identity to human GLX2, and has been cloned and overexpressed in *E. coli*.[10–12] Important findings of these studies include that: (1) GLX2 from *A. thaliana* can utilize either zinc, iron or manganese as the active site metal ion *in vivo*, (2) metal ion binding is influenced by both primary and secondary shell metal ligands, and (3) metal ion content for the enzyme depends on growth conditions. In addition, combined EPR, EXAFS, mass spectrometry and metal analysis studies indicate that metal coordination in GLX2 occurs in a non site-specific fashion and exclusively as dimetal centers that may be homogeneous or mixed-metal combinations (*e.g.* Fe(III)Fe(II), Fe(II)Fe(II), Mn(II)Mn(II), Fe(II)Mn(II), Fe(III)Zn(II), Mn(II)Zn(II), Fe(II)Zn(II) and Zn(II)Zn(II)).[11,12] Notably, similar levels of enzymatic activity are observed irrespective of the metal ion content. Finally, as no report exists to date in the literature of the metal ion content of a GLX2 enzyme purified from a native source, the specific *in vivo* metal ion content of GLX2 enzymes from various sources remains unclear.

Multiple aspects of the proposed chemistry of GLX2 enzymes remain to be fully investigated. For example, in a recent mechanistic proposal for *S*-D-lactolylglutathione hydrolysis by *A. thaliana* GLX2, Makaroff and coworkers proposed that interaction of the substrate with the active site metal centers induces the bridging hydroxide moiety to become terminal on M_2 prior to attack on the substrate.[10] This is consistent with proposed mechanisms for other binuclear hydrolases, such as leucine aminopeptidase,[13] but contrasts with the previously proposed mechanistic pathway for human GLX2 (Scheme 2).[6] Furthermore, it has been reported that product release occurs in an ordered fashion, with protonation and release first of lactic acid, followed by protonation of a metal-stabilized gluthione thiolate moiety and release of the free thiol.[10] This ordering indicates that the more basic thiolate is stabilized, perhaps through metal coordination. These issues, along with the impact of variable metal ion contents on the reaction pathway of GLX2 enzymes, remain to be fully examined.

In the work presented herein, we outline studies of the thioester cleavage reactivity of a series of zinc hydroxide complexes. While the first complex mimics some of the structural features of the active site binuclear metal center identified in the crystal structure of human GLX2, including the presence of a single bridging hydroxide ligand, it has been found to unreactive toward a model thioester substrate. A second type of binuclear complex, capable of forming mononuclear Zn–OH units in solution, does mediate the hydrolysis of a thioester substrate to give a zinc 2-hydroxyacid complex and free thiol.

Results and discussion

A binuclear zinc hydroxide complex of the 2,6-bis[(bis(2-pyridylmethyl)amino)methyl]-4-methylphenol (L^1H) ligand,[14] $[(L^1Zn_2)(\mu\text{-}OH)](ClO_4)_2$ (**1**, Fig. 2), was recently reported.[15] We independently prepared this complex *via* treatment of L^1H with $Zn(ClO_4)_2 \cdot 6H_2O$ in the presence of two equivalents of $(CH_3)_4NOH \cdot 5H_2O$, which yielded **1** in 82% yield following recrystallization from acetonitrile/diethyl ether (see supplementary information for details). Complex **1** was characterized by

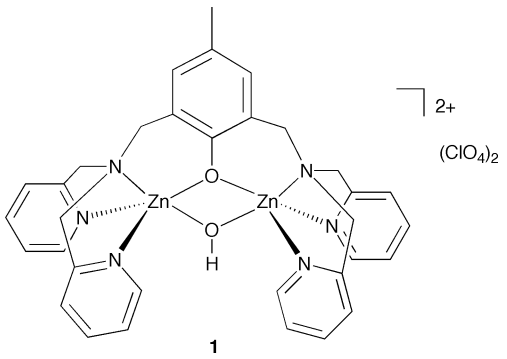

1

Fig. 2 Structural drawing of **1**.

X-ray crystallography, ^{1}H and ^{13}C NMR, IR spectroscopy, mass spectrometry, and elemental analysis.

A crystalline form of **1**, **1**·3CH_3CN, was obtained from acetonitrile–diethyl ether. This form belongs to the monoclinic crystal system and the $P2_1/c$ space group. In this structure, there are three molecules of acetonitrile per cation. This crystalline form differs from a previously reported crystalline sample of **1** (**1**·CH_3CN, triclinic, $P\bar{1}$) wherein there is one acetontrile molecule per cation.[15] We note that the overall quality of the structure of **1**·3CH_3CN ($R1/wR2 = 0.0488/0.0854$) is significantly better than that reported for **1**·CH_3CN ($R1/wR2 = 0.095/0.199$).[15] That being said, the metrical parameters for the cationic component of **1**·3CH_3CN are similar to those previously reported for **1**·CH_3CN.[15] For example, in each structure the zinc centers exhibit a distorted trigonal bipyramidal geometry.[16] In addition, in both structures, the Zn–O(H) distances (**1**·3CH_3CN: 1.984(2) and 1.985(2) Å; **1**·CH_3CN: 1.971(3) and 1.943(3) Å) are slightly shorter than the Zn–O(phenolate) distances (**1**·3CH_3CN: 2.0260(18) and 2.0511(19) Å; **1**·CH_3CN: 2.033(3) and 2.030(3) Å). The cationic portion of the X-ray structure of **1**·3CH_3CN is shown in Fig. S1 (ESI†). Details of the X-ray data collection and refinement for **1**·3CH_3CN are given in Table S1 (ESI†). Selected bond distances and angles are given in Table S2 (ESI†).

Important differences are apparent upon comparison of the structural features of the binuclear core of **1**·3CH_3CN with those of the active site metal cluster in GLX2.[6] For example, the metal ions in the protein exhibit a different overall geometry, having an approximately square pyramidal coordination environment in the absence of substrate. In addition, the M_1–O(Asp) interaction (2.2–2.6 Å) is much weaker than the M_2–O(Asp) interaction (2.0–2.2 Å). This asymmetry within the core, wherein the aspartate residue between the metal centers is essentially monodentate on M_2, is interesting and may be important in regard to reactivity of the bridging M–OH moiety. Specifically, in a proposed mechanism for thioester hydrolysis catalyzed by the GLX2 enzyme from *Arabidopsis thaliana*, Makaroff and coworkers have suggested that upon interaction of the thioester carbonyl oxygen with M_1 the bridging hydroxide moves to a terminal position on M_2.[10] In comparison, the core in **1**·3CH_3CN is symmetric, with identical Zn–O(H) distances that are on the short end of the range found in GLX2 (1.9–2.2 Å).[6] The M···M distance in the enzyme (3.3–3.5 Å) is significantly longer than that found in **1**·3CH_3CN (3.05 Å).

The acetonitrile solvate molecules found in the X-ray structure of **1**·3CH_3CN are lost upon drying of the bulk sample, ^{1}H and ^{13}C NMR studies of **1** in CD_3CN give the expected features, albeit a ^{1}H NMR resonance could not be identified for the bridging hydroxyl proton. Evidence for the hydroxide moiety is found in the solid state IR spectrum of **1**, wherein a broad O–H stretch is found at 3430 cm^{-1}. The broad nature of this feature may be due to hydrogen bonding involving a perchlorate anion. In this regard, in the X-ray structure of **1**·3CH_3CN, weak hydrogen bonding interactions are found between the hydroxyl proton and two perchlorate oxygen atoms (heteroatom distances: O(2)···O(9′) 3.024(8) Å, O(2)···O(10) 2.980(6) Å).

Reactivity studies of 1 with a thioester

The model thioester substrate hydroxyphenylthioacetic acid *S*-methyl ester was prepared in two steps according to literature procedures as shown in Scheme 3.[17,18] ^{1}H NMR analysis of the hemithioacetal product of reaction **A** (Scheme 3) revealed diagnostic –C*H*– and –SCH_3 resonances at 6.23 and 2.10 ppm, respectively, in CD_3CN. For the thioester product from reaction **B** (Scheme 3) these resonances are found at 5.23 and 2.21 ppm, respectively.

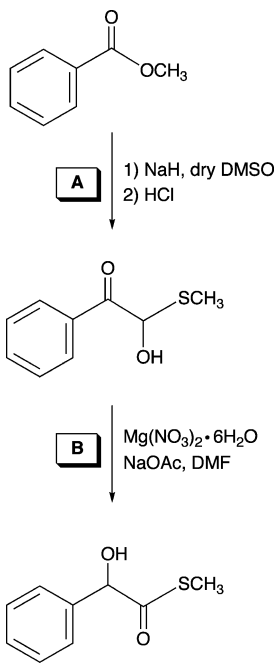

Scheme 3 Synthetic route used for the preparation of the thioester model substrate hydroxyphenylthioacteic acid *S*-methyl ester.[17,18]

Treatment of **1** with hydroxyphenylthioacetic acid *S*-methyl ester in CD_3CN at 45(1) °C for ~65 h resulted in no reaction as determined by ^{1}H NMR. Analysis of a space-filling model of the cationic portion of **1**·3CH_3CN (Fig. S2, ESI†) revealed that the zinc centers and bridging hydroxide moiety in this complex are exposed to solvent and thus accessible to interactions with the thioester molecule. We hypothesize that the lack of reactivity in this system is due to the poor nucleophilic character of the bridging hydroxide. However, weak binding of the thioester substrate to the zinc cation may also be an issue. In addition, we suspect that because of the symmetrical nature of the coordination

environment imparted by the L^1 chelate ligand, it is unlikely that the bridging hydroxide moiety will shift to a terminal position.

Synthesis and characterization of new $Zn_2(\mu\text{-}OH)_2$ complexes

As a portion of our study, we have also investigated thioester cleavage chemistry involving new binuclear zinc hydroxide complexes supported by N_3-donor type ligands. As shown in Schemes 4 and 5, two new N_3-donor ligands (L^2 and L^3), each having one internal hydrogen bond donor, have been constructed. Treatment of *N*-methyl-*N*-(2-pyridylmethyl)amine (Array Biopharma) with an equimolar amount of 2-pivaloylamido-6-bromomethylpyridine,[19] followed by reduction of the amide-containing ligand precursor using $LiAlH_4$, gave L^2 in modest yield (Scheme 4). The L^3 ligand was also prepared *via* $LiAlH_4$ reduction of an amide-appended precursor (Scheme 5).[20]

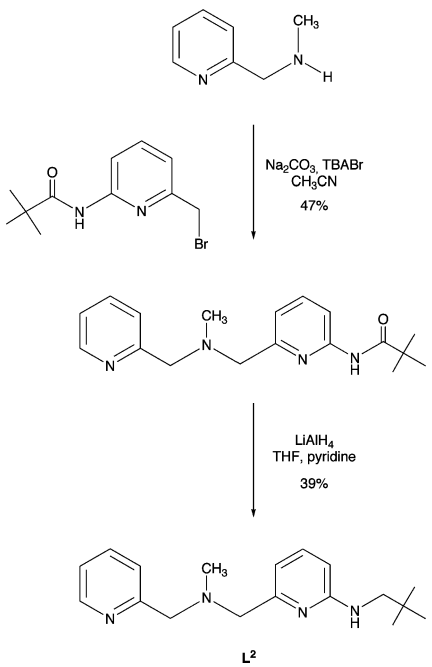

Scheme 4 Synthesis of L^2 ligand.

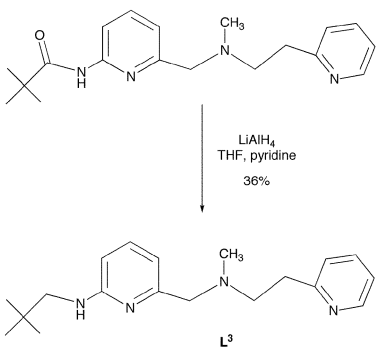

Scheme 5 Synthesis of L^3 ligand from amide-appended precursor.[20]

Treatment of L^2 or L^3 with equimolar amounts of $Zn(ClO_4)_2 \cdot 6H_2O$ and KOH in CH_3OH, followed by recrystallization from CH_3CN–Et_2O (L^2) or CH_3CN–CH_2Cl_2–Et_2O (L^3), yielded crystals suitable for single-crystal X-ray crystallography. The hydroxide complexes, $[(L^2Zn)_2(\mu\text{-}OH)_2](ClO_4)_2$ (**2**) and $[(L^3Zn)_2(\mu\text{-}OH)_2](ClO_4)_2 \cdot 0.5CH_3CN$ (**3**), have also been characterized by ^1H and ^{13}C NMR, FTIR, and elemental analysis.

The cationic portions of **2**·CH_3CN and **3**·$0.5CH_2Cl_2$·$0.5CH_3CN$ are shown in Fig. 3. Information concerning the X-ray data acquisition and refinement is given in Table 1. Selected bond distances and angles for **2**·CH_3CN and **3**·$0.5CH_2Cl_2$·$0.5CH_3CN$ are presented in Table 2.

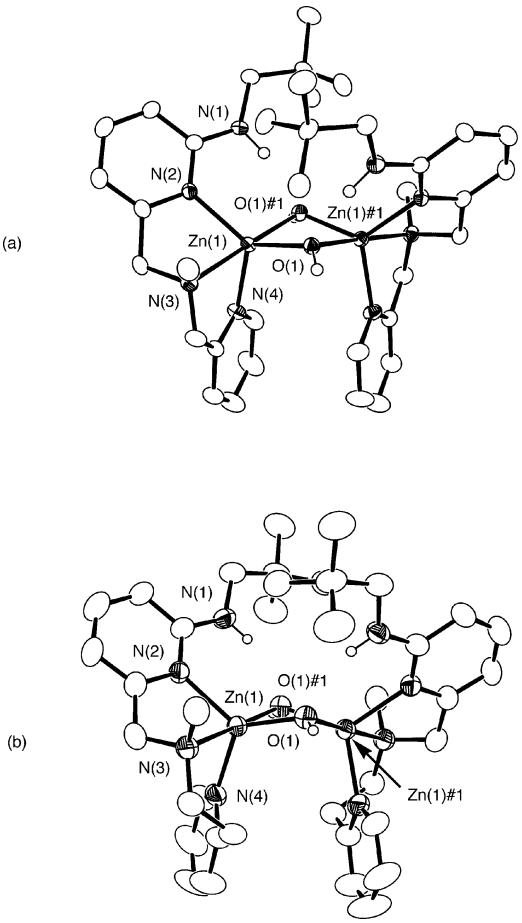

Fig. 3 ORTEP drawings of the cationic portions of **2**·CH_3CN and **3**·$0.5CH_2Cl_2$·$0.5CH_3CN$. All hydrogen atoms, except the hydroxyl and secondary amine protons, have been omitted for clarity. Ellipsoids are drawn at the 50% probability level for **2**·CH_3CN and at the 35% probability level for **3**·$0.5CH_2Cl_2$·$0.5CH_3CN$.

The cationic portions of **2**·CH_3CN and **3**·$0.5CH_2Cl_2$·$0.5CH_3CN$ are comprised of a binuclear $Zn_2(\mu\text{-}OH)_2$ core supported at each zinc center by a N_3-donor ligand. The core has a hinge-type distortion wherein each bridging hydroxide oxygen atom accepts a hydrogen bond from the secondary amine group of the supporting chelate ligand. These secondary interactions may be classified as moderate hydrogen bonds on the basis of the heteroatom bond distances and angles (**2**·CH_3CN: N(1)···O(1)#1 2.852(4) Å, N(1)–H(1N)···O(1)#1 164(4)°; **3**·$0.5CH_2Cl_2$·$0.5CH_3CN$: N(1)···O(1) 2.864(6) Å, N(1)–H(1N)···O(1) 158(4)°).[21] Each hydroxyl proton is also involved in a hydrogen bonding interaction with an oxygen atom of a perchlorate anion. The hinge-type core found in **2**·CH_3CN and

Table 1 Summary of X-ray data collection and refinement for **2**·CH_3CN and **3**·0.5CH_2Cl_2·0.5CH_3CN[a]

	2·CH_3CN	**3**·0.5CH_2Cl_2·0.5CH_3CN
Empirical formula	$C_{40}H_{60}Cl_2N_{10}O_{10}Zn_2$	$C_{39.50}H_{60.50}Cl_3N_{8.50}O_{10}Zn_2$
M	1042.62	1051.55
Crystal system	Monoclinic	Tetragonal
Space group	C_2/c	$P4_322$
a/Å	16.5217(3)	11.4472(7)
b/Å	16.3421(2)	11.4472(7)
c/Å	19.4004(4)	37.628(2)
β/°	112.8344(8)	90
V/Å^3	4827.58(15)	4930.8(5)
Z	4	4
D_c/Mg m^{-3}	1.435	1.417
T/K	150(1)	150(1)
Color	Colorless	Colorless
Crystal size/mm	0.25 × 0.25 × 0.23	0.33 × 0.28 × 0.25
Diffractometer[a]	Nonius KappaCCD	Nonius KappaCCD
μ/mm^{-1}	1.168	1.196
$2\theta_{max}$/Å	54.94	55.00
Completeness to $\theta = 27.94°$ (%)	99.7	96.7
Reflections collected	9712	9994
Independent reflections	5522	5428
R_{int}	0.0185	0.0433
Variable parameters	330	300
$R1/wR2$[b]	0.0540/0.1267	0.0556/0.1034
Goodness-of-fit (F^2)	1.220	1.100
$\Delta\rho_{max\ min}$/e Å^{-3}	0.490/−0.567	0.482/−0.602

[a] Radiation used: Mo-Kα ($\lambda = 0.71073$ Å). [b] $R1 = \sum\|F_o| - |F_c\|/\sum|F_o|$; $wR2 = [\sum[w(F_o^2\text{-}F_c^2)^2]/[\sum(F_o^2)^2]]^{1/2}$ where $w = 1/[\sigma^2(F_o^2) + (aP)^2 + bP]$.

Table 2 Selected bond lengths (Å) and angles (°) for **2**·CH_3CN and **3**·0.5CH_2Cl_2·0.5CH_3CN[a]

2·CH_3CN			
Zn(1)–O(1)	1.983(3)	Zn(1)–N(3)	2.105(3)
Zn(1)–O(1)#1	2.038(3)	Zn(1)–N(4)	2.225(3)
Zn(1)–N(2)	2.079(3)	Zn(1)···Zn(1)#1	2.9838(8)
O(1)–Zn(1)–O(1)#1	80.32(12)	N(2)–Zn(1)–N(4)	119.83(12)
O(1)–Zn(1)–N(2)	126.53(11)	O(1)–Zn(1)–N(3)	99.75(11)
O(1)#1–Zn(1)–N(2)	101.33(11)	O(1)#1–Zn(1)–N(3)	178.39(11)
O(1)–Zn(1)–N(4)	111.88(12)	N(2)–Zn(1)–N(3)	79.95(11)
O(1)#1–Zn(1)–N(4)	101.28(11)	N(4)–Zn(1)–N(3)	77.20(12)
3·0.5CH_2Cl_2·0.5CH_3CN			
Zn(1)–O(1)	2.070(3)	Zn(1)–N(3)	2.243(4)
Zn(1)–O(1)#1	1.963(3)	Zn(1)–N(4)	2.099(4)
Zn(1)–N(2)	2.079(4)	Zn(1)···Zn(1)#1	2.9871(10)
O(1)–Zn(1)–O(1)#1	79.10(17)	N(2)–Zn(1)–N(4)	113.77(15)
O(1)–Zn(1)–N(2)	100.20(14)	O(1)–Zn(1)–N(3)	178.12(16)
O(1)#1–Zn(1)–N(2)	125.78(14)	O(1)#1–Zn(1)–N(3)	99.26(15)
O(1)–Zn(1)–N(4)	95.50(15)	N(2)–Zn(1)–N(3)	79.99(15)
O(1)#1–Zn(1)–N(4)	120.30(15)	N(4)–Zn(1)–N(3)	86.11(16)

[a] Estimated standard deviations indicated in parentheses.

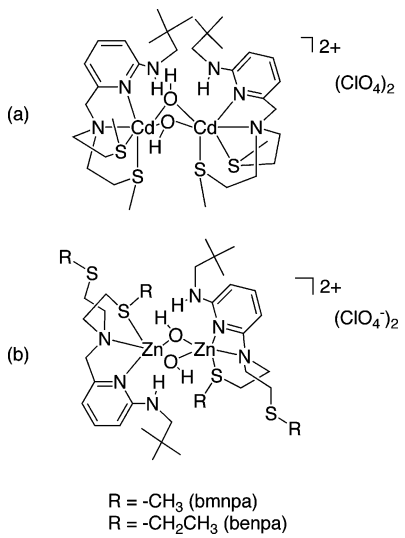

Fig. 4 Structural drawings of (a) [(bmnpaCd)$_2$(μ-OH)$_2$](ClO$_4$)$_2$ and (b) [(bmnpa/benpaZn)$_2$(μ-OH)$_2$](ClO$_4$)$_2$.[22,25,26]

3·0.5CH_2Cl_2·0.5CH_3CN is similar to that found in [(bmnpaCd)$_2$(μ-OH)$_2$](ClO$_4$)$_2$ (bmnpa = *N*,*N*-bis-2-(methylthio)ethyl-*N*-((6-neopentylamino-2-pyridyl)methyl)amine) (Fig. 4(a)).[22] In this binuclear cadmium hydroxide complex, the positioning of both neopentyl amino substituents on one side of the Cd$_2$(μ-OH)$_2$ core results in CH/π interactions between the neopentyl hydrogens of one chelate ligand and the pyridyl ring of the other chelate ligand.[23,24] These interactions are characterized by methyl or methylene carbon/arene centroid distances of 3.15–3.84 Å. In the solid-state structures of **2**·CH_3CN and **3**·0.5CH_2Cl_2·0.5CH_3CN, the shortest methyl carbon/arene centroid distances are 4.06 and 4.34 Å, respectively. As these distances exceed the sum of the van der Waals radii of a methyl group and a C_{sp^2} unit (3.7 Å),[24] no CH/π interactions are present in the solid-state structures of **2**·CH_3CN and **3**·0.5CH_2Cl_2·0.5CH_3CN.

The symmetry-related zinc centers in **2**·CH_3CN and **3**·0.5CH_2Cl_2·0.5CH_3CN exhibit a distorted trigonal bipyramidal geometry ($\tau = 0.86$, **2**·CH_3CN; $\tau = 0.87$, **3**·0.5CH_2Cl_2·0.5CH_3CN) with two pyridyl nitrogens and a hydroxide oxygen atom occupying equatorial positions.[16] The Zn···Zn distances (2.9838(8),

2.9871(10) Å) are comparable to the Zn···Zn distances in the binuclear zinc hydroxide derivatives $[(bmnpaZn)_2(\mu\text{-}OH)_2](ClO_4)_2$ (2.98 Å)[25] and $[(benpaZn)_2(\mu\text{-}OH)_2](ClO_4)_2$ (2.97 Å; benpa = *N*,*N*-bis-2-(ethylthio)ethyl-*N*-((6-neopentylamino-2-pyridyl)methyl)amine) (Fig. 4(b)).[26] Two slightly different Zn–O(H) distances are found within the cationic portions of **2**·CH_3CN and **3**·$0.5CH_2Cl_2$·$0.5CH_3CN$. These distances (Table 2) are within the range (1.9–2.3 Å) previously reported for bridging hydroxide ligands in multinuclear zinc complexes.[25] Similar to the core structures of $[(bmnpaZn)_2(\mu\text{-}OH)_2](ClO_4)_2$ and $[(benpaZn)_2(\mu\text{-}OH)_2](ClO_4)_2$, in **2**·$CH_3CN$ and **3**·$0.5CH_2Cl_2$·$0.5CH_3CN$, the longer Zn–O(H) distance involves the oxygen atom that accepts a hydrogen bond from the supporting chelate ligand on the same zinc center.

In CH_3CN solution, analytically pure samples of **2** and **3** behave as 1 : 1 electrolytes, thus indicating a breakup of the binuclear cations in these complexes into $[(L^2/L^3)Zn\text{–}OH]ClO_4$ fragments. This is evident from the Onsager slopes exhibited by these complexes in CH_3CN solution, as shown in Fig. 5, which are similar to that of the 1 : 1 electrolyte standard Me_4NClO_4. For comparison, the conductance data for $[(bmnpaZn)_2(\mu\text{-}OH)_2](ClO_4)_2$[25] is also shown in Fig. 5. The higher slope value for this complex indicates the presence of a 1 : 2 electrolyte.[27]

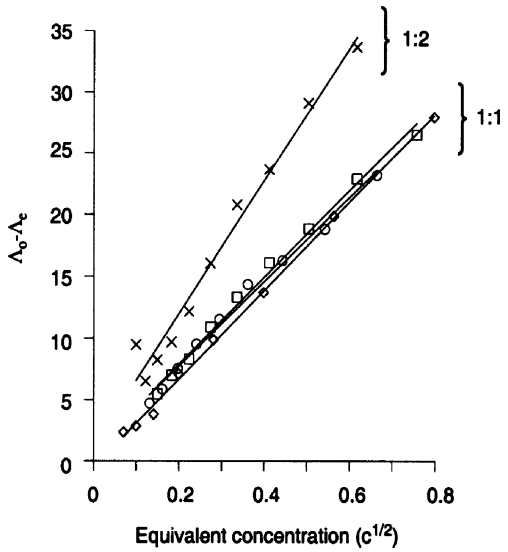

Fig. 5 Onsager plots for $[(bmnpaZn)_2(\mu\text{-}OH)_2](ClO_4)_2$;[25] (×), **2** (□), **3** (○) and Me_4NClO_4 (◇).

The ^{1}H NMR features of analytically pure **2** in dry CD_3CN at ambient temperature are sharp and indicative of the presence of a major and minor species at ambient temperature (Fig. S3(a), ESI†). For the major species, a sharp N–H resonance is present at 9.18 ppm. This signal appears as a triplet (J = 5.2 Hz) due to coupling with the adjacent methylene protons in the neopentyl portion of the L^2 ligand. This observed coupling, along with the deshielding of the N–H proton resonance, provides evidence for the involvement of the secondary amine N–H in a hydrogen bonding interaction.[21] Based on the solid state X-ray structure of **2**·CH_3CN and the above-mentioned conductance experiments, we propose that this hydrogen bonding interaction involves the Zn–OH moiety of a mononuclear $[(L^2)Zn\text{–}OH]ClO_4$ species in solution. Additionally, the protons of the benzylic positions of the major species are diastereotopic, appearing as four doublets in the chemical shift range of 3.4–4.5 ppm. The neopentyl methylene protons of the major species appear as a doublet of doublets. The magnitude of the coupling constants in this signal indicates that these protons are diastereotopic and each coupled to the secondary amine N–H proton. The minor species present in dry CD_3CN solutions of **2** has a *tert*-butyl methyl signal at 0.77 ppm and remains to be conclusively identified. However, based on the fact that a binuclear cation is present in the solid state structure of **2**·CH_3CN, we propose that the minor species may be a binuclear form of the complex.

The ^{1}H NMR features of analytically pure **3** in dry CD_3CN (Fig. S3(b), ESI†) at ambient temperature also indicate the presence of two species, albeit the ratio is different than that found for **2**. The major and minor species for **3** have secondary amine N–H resonances at 9.24 and 9.06 ppm, respectively. Integration of these signals provides a ratio of ~2 : 1 for the major *vs*. minor species. The *tert*-butyl methyl resonance for the minor species (0.85 ppm) is again upfield of that of the major species (0.90 ppm). Speculating that these two species may be mono- and binuclear forms of **3**, we investigated CD_3CN solutions of **3** using ^{1}H NMR at variable temperatures and concentrations. Both heating and cooling produced peak broadening that prevented careful integration of the individual resonances. Examination of the ^{1}H NMR features of **3** in CD_3CN over a ten-fold concentration range (1.8×10^{-2}–1.8×10^{-3} M) produced a subtle change (~6%) in the ratio of the integrated intensities of the *tert*-butyl resonances of the two species. However, as these resonances overlap at the baseline, we are hesitant to assign significance to this observed change. The conductance experiments for **3** (Fig. 5) were performed over a concentration range of 4.9×10^{-3}–1.3×10^{-4} M. As the results of these measurements indicate the presence of a 1 : 1 electrolyte, we propose that the major species present in acetonitrile solutions of **3** is a mononuclear $[(L^3)Zn\text{–}OH]ClO_4$ species and that this species becomes more dominant as the concentration decreases.

Thioester hydrolysis reactivity of 2 and 3

Treatment of **2** or **3** with one equivalent of hydroxyphenylthioacetic acid *S*-methyl ester per Zn–OH moiety for 3 h at 45 °C in acetonitrile results in the clean formation of new zinc complexes (Scheme 6). The complexes, designated **4** and **5**, have been isolated as powdered solids and have been characterized by elemental

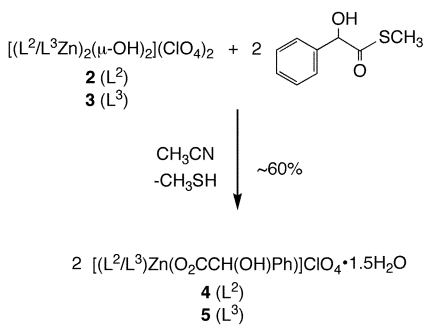

Scheme 6 Reactivity of **2** and **3** with hydroxyphenylthioacetic acid *S*-methyl ester.

analysis, conductance measurements, and ^{1}H and ^{13}C NMR and IR spectroscopy. Attempts to generate crystalline samples of **4** and **5** suitable for X-ray crystallography have thus far failed.

Combustion elemental analysis data for **4** and **5** is consistent with the empirical formulas $[(L^2)Zn(O_2CCH(OH)Ph)]ClO_4\cdot 1.5H_2O$ and $[(L^3)Zn(O_2CCH(OH)Ph)]ClO_4\cdot 1.5H_2O$, respectively, for these complexes. The presence of water in the powdered samples sent for elemental analysis was confirmed by evaluation of the samples by ^{1}H NMR in dry CD_3CN. Although the solid state structures of **4** and **5** are unknown, conductance measurements (Fig. 6), performed using analytically pure samples, indicate that both complexes behave as 1 : 1 electrolytes in CH_3CN solution. Notably, a search of the Cambridge Crystallographic Database (CSD version 5.26 (updated May 2005)) revealed only one example of a zinc complex having a coordinated mandelate ($O_2CCH(OH)Ph$) anion.[28] This complex has two monodentate α-hydroxycarboxylate ligands.

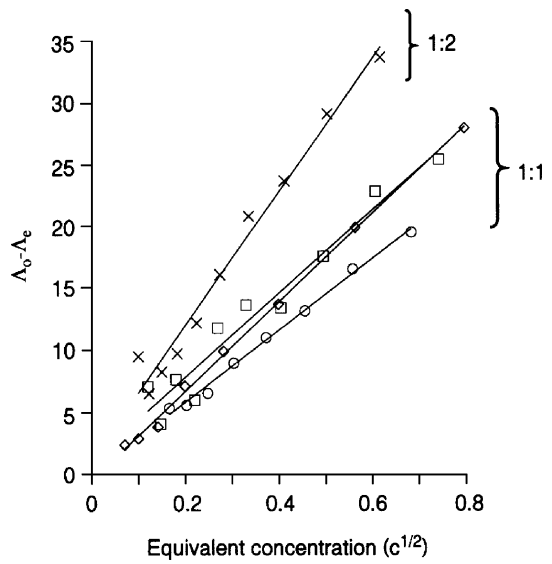

Fig. 6 Onsager plots for $[(bmnpaZn)_2(\mu\text{-}OH)_2](ClO_4)_2$;[25] (×), **4** (□), **5** (○) and Me_4NClO_4 (◇).

The ^{1}H NMR resonances of **4** and **5** in dry CD_3CN are generally sharp. However, for both complexes, two broad signals are found in the range of 4–7 ppm (**4**: 5.45 and 6.49 ppm; **5**: 4.58 and 6.82 ppm). These signals disappear in the presence of D_2O and thus are likely the mandelate hydroxyl proton and secondary amine proton resonances. In the ^{13}C NMR spectra of **4** and **5**, the carboxylate carbon centers exhibit resonances at 178.7 and 179.8 ppm, respectively. The IR features of **4** and **5** related to the mandelate hydroxyl group and zinc-bound carboxylate moiety are not easily interpreted. This is because the regions of ~3400–3200 and ~1650–1400 cm^{-1} also contain vibrations associated with the supporting L^2 and L^3 chelate ligands. The presence of ClO_4^- in analytically pure samples of **4** and **5** is evident from vibrations at ~1100 and 625 cm^{-1}. In sum, despite the lack of X-ray crystallographic characterization for **4** or **5**, analytical, conductance, and spectroscopic data are consistent with the empirical formulation of these complexes as $[(L^2/L^3)Zn(O_2CCH(OH)Ph)]ClO_4\cdot 1.5H_2O$.

Formation of the carboxylate derivatives **4** and **5** as shown in Scheme 6 requires the release of CH_3SH. We first attempted to identify CH_3SH production in the reaction mixture using ^{1}H NMR. However, as this volatile compound has a $-SCH_3$ resonance at ~2.0 ppm, a region that is obscured by the residual solvent resonance in CD_3CN, we instead used the deuterated analog, hydroxyphenylthioacetic acid *S*-methyl(d_3) ester. This compound, which was prepared using the procedure outlined in Scheme 4 starting from d_6-DMSO, enables the use of ^{2}H NMR as a technique to detect CD_3SH production in protioacetonitrile. A reaction mixture containing **3** and hydroxyphenylthioacetic acid *S*-methyl(d_3) ester in CH_3CN initially exhibited a single ^{2}H NMR resonance at 2.35 ppm when referenced to an internal standard of CD_3NO_2. However, within minutes at ambient temperature, a new ^{2}H NMR resonance is present at 2.02 ppm. This resonance disappears if the tube is opened, indicating the formation of a volatile product.

Conclusions

In this study, we have performed an initial evaluation of the thioester cleavage reactivity of three zinc hydroxide complexes. To our knowledge, this work provides the first examples of zinc hydroxide-mediated thioester hydrolysis.[29,30] Conclusions with relevance to GLX2 can be drawn from this initial study. First, as the hydroxide moiety in **1**, which symmetrically bridges two structurally similar Zn(II) centers, is not sufficiently nucleophilic to react with a thioester substrate, it seems likely that a terminal or quasi-terminal metal hydroxide moiety may be required for the hydrolysis of a thioester substrate. This notion supports a proposed mechanism put forth by Makaroff and co-workers for GLX2 wherein a terminal hydroxide on M_2 attacks the thioester substrate.[10] Notably, we have found that zinc hydroxide complexes that dissociate into mononuclear terminal $[(L)Zn\text{–}OH]ClO_4$ species in CH_3CN solution (**2** and **3**) are reactive for the hydrolysis of a thioester. While kinetic studies are needed to elucidate the reactive form of the complex, in this work we have identified the reaction products as zinc mandelate complexes and CH_3SH. The production of free thiol in these systems indicates that the more basic thiolate anion (*vs.* the carboxylate product) becomes protonated upon thioester cleavage.

In terms of the possible requirement of a terminal hydroxide for thioester cleavage, we note that studies of another dinuclear metallohydrolase, purple acid phosphatase,[31,32] suggest that a terminal or quasi-terminal metal hydroxide is required for the hydrolysis of a phosphate ester substrate. However, these results contrast with results of ENDOR studies of uterferrin, which suggest the involvement of a bridging hydroxide as the required nucleophile.[33] Recent studies of the reactivity of dizinc complexes of varying Zn···Zn distance with a phosphate diester substrate revealed that hydrolytic reactivity increased with a larger Zn···Zn separation. This was attributed to the formation of a quasi-terminal Zn–OH species (Zn–OH···HO(H)–Zn).[34] Overall, the question of whether a terminal or bridging hydroxide is the active nucleophile for substrate hydrolysis remains under investigation for a variety of binuclear metallohydrolases.

Finally, it is important to note that detailed mechanistic studies of thioester hydrolysis by GLX2 have been limited by the aforementioned heterogeneity of enzyme samples in terms of metal

ion content for enzyme produced recombinantly in *Escherichia coli*.[11] In light of this limitation, this is an ideal area for the use of synthetic model studies to carefully address how varying metal ion compositions influence the mechanistic pathway of thioester hydrolysis. In addition, synthetic model studies can also be used to address how the differing metal coordination environments in GLX2 influence the reactivity of a bridging hydroxide moiety. Building on the initial results presented in this study, efforts are underway in our laboratory in pursuit of these goals.

Experimental

General

All reagents and solvents were obtained from common commercial sources and were used as received unless otherwise noted. Solvents were dried according to published procedures and were distilled under N_2 prior to use.[35] Air sensitive procedures were performed in a MBraun Unilab glovebox under an atmosphere of purified N_2. IR spectra were recorded on a Shimadzu FTIR-8400 as KBr pellets. ^{1}H and ^{13}C{^{1}H} NMR spectra for characterization purposes were recorded in dry CD_3CN at ambient temperature on a JEOL 270 MHz or Bruker ARX400 spectrometer. Chemical shifts (in ppm) are referenced to the residual solvent peak(s) in C*H*D$_2$CN (^{1}H: 1.94 (quintet); ^{13}C{^{1}H}: 1.39 (heptet) ppm). ^{2}H NMR spectra were recorded as previously described.[36] Conductance measurements were performed and analyzed using methods that have been previously described.[22] Electron impact and fast atom bombardment mass spectra were obtained at the University of California, Riverside. Elemental analyses were performed by Atlantic Microlabs of Norcross, GA.

The protonated form of 2,6-bis[(bis(2-pyridylmethyl)amino)-methyl]-4-methylphenol (L^{1}H), and the ligand precursor 2-pivaloylamido-6-bromomethylpyridine, were prepared according to literature procedures.[14,19] *N*-Methyl-*N*-(2-pyridylmethyl)amine hydrochloride was purchased from Array Biopharma and was used as received. *N*-methyl-*N*-((6-pivaloylamido-2-pyridyl)-methyl)-*N*-(2-pyridylethyl)amine was prepared as previously described.[20] The model thioester substrate hydroxyphenylthioacetic acid *S*-methyl ester was prepared according to literature procedures.[17,18]

CAUTION: Perchlorate salts of metal complexes with organic ligands are potentially explosive. Only small amounts of material should be prepared and these should be handled with great care.[37]

Synthesis of ligands and complexes

***N*-Methyl-*N*-((6-pivaloylamido-2-amino)methyl)-*N*-((2-pyridyl)-methyl)amine.** To a solution of *N*-methyl-*N*-(2-pyridylmethyl)-amine (0.17 g, 0.89 mmol) in CH_3CN (30 mL) was added 2-pivaloylamido-6-bromomethylpyridine (0.24 g, 0.89 mmol), sodium carbonate (0.48 g, 4.5 mmol), and tetrabutylammonium bromide (~2 mg). This mixture was heated at reflux under N_2 for 15 h. After the solution was cooled to room temperature, 1 M NaOH (30 mL) was added and the entire solution was transferred to a separation funnel. The aqueous/acetonitrile sample was extracted with CH_2Cl_2 (3 × 30 mL). All organic fractions were then combined and dried over Na_2SO_4. Filtration, followed by removal of solvent under reduced pressure, yielded a yellow–brown oil. Purification of this oil (R_f ~ 0.75, broad trailing band) by column chromatography on silica gel using methanol as the eluent yielded a pale yellow oil (0.13 g, 47%); ν_{max}/cm^{-1}: (NH) 3340 (br), (C=O) 1689; δ_H (400 MHz, solvent CD_3CN): 1.27 (9H, s), 2.22 (3H, s), 3.61 (2H, s), 3.70 (2H, s), 7.16–7.21 (1H, m), 7.25 (1H, d, J = 7.5 Hz), 7.51 (1H, d, J = 7.8 Hz), 7.70 (2H, t, J = 7.8 Hz), 7.99 (1H, d, J = 8.2 Hz), 8.20 (1H, br, N–H), 8.48 (1H, d, J = 4.2 Hz); δ_C (100 MHz, solvent CD_3CN): 27.6, 40.5, 43.0, 64.0, 64.4, 112.8, 119.6, 123.1, 123.9, 137.4, 139.6, 150.0, 152.4, 159.3, 160.6, 178.0 (16 signals expected and observed).

***N*-Methyl-*N*-((6-neopentylamino-2-pyridyl)methyl)-*N*-((2-pyridyl)methyl)amine (L^2).** To a mixture of dry pyridine (3 mL) and dry THF (12 mL) was added $LiAlH_4$ (0.075 g, mmol). To this solution was added a THF solution of *N*-methyl-*N*-((6-pivaloylamido-2-amino)methyl)-*N*-((2-pyridyl)methyl)amine (0.13 g, 0.42 mmol; ~10 mL THF) in a dropwise manner. The resulting solution was heated at reflux for 48 h, at which point it was cooled to room temperature and water was added dropwise until no bubbling was observed. Extraction of this solution with ethyl acetate (3 × 50 mL), followed by drying of the combined organic fractions over sodium sulfate, filtration, and removal of the solvent under reduced pressure yielded the product as a brown oil. Purification of this oil (R_f ~0.8, broad trailing band) *via* column chromatography on silica gel using methanol as the eluent yielded a pale yellow oil (0.048 g, 39%); δ_H (400 MHz, solvent CD_3CN): 0.92 (9H, s), 2.27 (3H, s), 2.75–2.79 (2H, m), 2.92–2.96 (2H, m), 3.11 (2H, d, J = 6.3 Hz), 3.44 (2H, s), 4.95 (1H, br, N–H), 6.31 (1H, d, J = 8.2 Hz), 6.45 (1H, d, J = 7.4 Hz), 7.11–7.15 (1H, m), 7.22 (1H, d, J = 7.9 Hz), 7.29 (1H, t, J = 8.2 Hz), 8.44 (1H, d, J = 5.6 Hz); δ_C (100 MHz, solvent CD_3CN): 27.0, 33.0, 43.1, 52.0, 64.3, 64.5, 106.3, 111.8, 122.0, 123.5, 137.4, 138.4, 149.6, 158.4, 160.4, 160.9 (16 signals expected and observed); EI-MS: m/z 299 (MH$^+$, 65%).

***N*-Methyl-*N*-((6-neopentylamino-2-pyridyl)methyl)-*N*-((2-pyridyl)ethyl)amine (L^3).** Prepared *via* $LiAlH_4$ reduction of *N*-methyl-*N*-((6-pivaloylamido-2-pyridyl)methyl)-*N*-((2-pyridyl)-ethyl)amine (mpppa)[20] using experimental methods identical to those employed for the preparation and isolation of L^2 (yield: 36%); δ_H (270 MHz, solvent CD_3CN): 0.92 (9H, s), 2.26 (3H, s), 2.73–2.78 (2H, m), 2.90–2.96 (2H, m), 3.44 (s, 2H), 4.96 (1H, br, N–H), 6.31 (1H, d, J = 8.2 Hz), 6.44 (1H, d, J = 7.4 Hz), 7.12–7.18 (m, 1H), 7.21 (1H, d, J = 7.6 Hz), 7.60–7.64 (m, 1H), 8.44 (1H, d, J = 5.6 Hz); δ_C (100 MHz, solvent CD_3CN): 28.0, 32.9, 36.7, 43.4, 53.7, 58.1, 64.4, 106.0, 111.7, 122.0, 124.4, 136.9, 138.2, 149.9, 158.4, 160.1, 161.7 (17 signals expected and observed); EI-MS: m/z 312 (M$^+$, 10%).

[(L^{2}Zn)$_2$(μ-OH)$_2$](ClO$_4$)$_2$ (2). To a methanol solution of L^2 (57 mg, 0.19 mmol) was added a methanol solution of $Zn(ClO_4)_2 \cdot 6H_2O$ (70 mg, 0.19 mmol). The total volume of the resulting solution was ~6 mL. After stirring for ~5 min, this solution was added to a methanol solution of KOH (11 mg, 0.19 mmol, ~3 mL CH_3OH). The resulting mixture was stirred for 12 h at ambient temperature, at which point a white solid had deposited on the bottom of the reaction vessel. The organic solvent was carefully decanted from this solid. The white solid was then dissolved in CH_3CN (~10 mL) and the solution was filtered through a Celite/glass wool plug. The filtrate was then pumped to

dryness and the remaining solid was recrystallized from CH_3CN *via* Et_2O diffusion at room temperature (75 mg, 82%) (Found: C, 44.60; H, 5.75; N, 11.57. $C_{36}H_{54}N_8Zn_2Cl_2O_{10}$ requires C, 45.18; H, 5.69; N, 11.72%); ν_{max}/cm^{-1}: (OH) 3600, (NH) 3214, (ClO_4) 1111, (ClO_4) 624 (KBr); δ_H (400 MHz, solvent CD_3CN): 0.91 (9H, s), 2.60 (3H, s), 2.85 (1H, dd, $J_1 = 12$ Hz, $J_2 = 5.2$ Hz), 2.97 (1H, dd, $J_1 = 12$ Hz, $J_2 = 5.2$ Hz), 3.42 (1H, d, $J = 14$ Hz), 3.58 (1H, d, $J = 14$ Hz), 4.10 (1H, d, $J = 16.7$ Hz), 4.38 (1H, d, $J = 16.7$ Hz), 6.55 (1H, d, $J = 7.2$ Hz), 6.61 (1H, d, $J = 8.8$ Hz), 7.63 (1H, m), 7.83 (1H, t, $J = 7.7$ Hz), 8.18 (1H, d, $J = 5.2$ Hz), 9.19 (1H, t, $J = 5.2$ Hz, NH); δ_C (100 MHz, solvent CD_3CN): 27.9, 32.4, 43.7, 55.8, 59.5, 60.5, 108.1, 112.0, 125.3, 125.7, 142.0, 142.4, 148.6, 153.2, 155.7, 161.7 (16 signals expected and observed).

$[(L^3Zn)_2(\mu\text{-}OH)_2](ClO_4)_2\cdot 0.5CH_3CN$ (3). Prepared and characterized in an identical manner to **2** (yield: 54%). Recrystallization of this complex *via* diethyl ether diffusion into a CH_3CN–CH_2Cl_2 (1 : 1) solution yielded a white crystalline material suitable for single-crystal X-ray analysis (Found: C, 47.05; H, 6.15; N, 12.32. $C_{39}H_{59.5}N_{8.5}Zn_2Cl_2O_{10}$ requires: C, 46.58; H, 5.97; N, 11.85%); ν_{max}/cm^{-1}: (OH) 3600, (NH) 3229, (ClO_4) 1098, (ClO_4) 624 (KBr); Two species (ratio ~2 : 1) are indicated by ^1H NMR in CD_3CN solutions of analytically pure **3** at 25(1) °C (see Fig. S3(b), ESI†). Diagnostic ^1H NMR signals for the major species include δ_H (400 MHz, solvent CD_3CN): 0.94 (9H, s), 2.42 (3H, s), 6.42 (1H, d, $J = 6.9$ Hz), 6.62 (1H, d, $J = 8.7$ Hz), 7.22 (1H, d, $J = 7.8$ Hz), 8.53 (1H, d, $J = 5.1$ Hz), 9.23 (1H, br, NH); Diagnostic signals for minor species include δ_H (400 MHz, solvent CD_3CN): 0.85 (9H, s), 2.46 (3H, s), 6.48 (1H, d, $J = 7.4$ Hz), 6.55 (1H, d, $J = 8.8$ Hz), 8.61 (1H, d, $J = 4.8$ Hz), 9.06 (1H, br, NH).

General procedure for the reaction of 2 and 3 with hydroxyphenylthioacetic acid *S*-methyl ester. Preparation of $[(L^2)Zn(O_2CCH(OH)Ph)](ClO_4)_2\cdot 1.5H_2O$ (4) and $[(L^3)Zn(O_2CCH(OH)Ph)](ClO_4)_2\cdot 1.5H_2O$ (5). To a solution of **2** or **3** (0.1 mmol) in acetonitrile (12 mL) was added hydroxyphenylthioacetic acid *S*-methyl ester (0.2 mmol) and the resulting mixture was heated at 45(1) °C for 3 h. At this point, the heat was removed and the solution was filtered through a Celite/glass wool plug. Et_2O diffusion into the CH_3CN solution resulted in the deposition of a white powder in a pale yellow solution. The solution was then decanted from the solid. Addition of excess Et_2O to the yellow filtrate at ambient temperature resulted in each case in the deposition of an oily compound that became solid after drying under vacuum (yield: ~60%). **4** (Found: C, 48.75; H, 5.28; N, 8.73. $C_{25}H_{33}N_4ZnClO_7\cdot 1.5H_2O$ requires C, 48.69; H, 5.66, N, 8.73%; ν_{max}/cm^{-1}: (NH(OH) ~3390, (ClO_4) 1108, (ClO_4) 625 (KBr); δ_H (400 MHz, solvent CD_3CN): 0.89 (9H, s), 2.19 (3H, s), 2.78–2.84 (2H, m), 3.70–3.80 (2H, m), 3.96 (2H, br s), 4.99 (1H, br s), 5.45 (1H, br), 6.49 (1H, br), 6.57 (1H, d, $J = 7.1$ Hz), 6.64 (1H, d, $J = 8.7$ Hz), 7.10–7.25 (5H, m), 7.30–7.36 (1H, m), 7.46 (1H, d, $J = 7.8$ Hz), 7.62–7.66 (1H, m), 7.98–8.01 (1H, m), 8.20 (1H, br s) (addition of D_2O results in loss of the signals at 5.44 and 6.49 ppm and appearance of coupling in the signals at 3.70–3.80 and 3.96 ppm); δ_C (100 MHz, solvent CD_3CN): 27.6, 32.8, 43.4, 55.0, 60.9, 61.5, 74.5, 108.0, 112.2, 125.4, 126.0, 127.8, 128.9, 129.3, 141.9, 142.3, 148.7, 152.5, 155.1, 160.4, 178.7 (22 signals expected, 21 observed; 1 aromatic resonance not observed, presumably due to overlap); FAB-MS: m/z 513 ($[M - ClO_4 - 1.5H_2O]^+$, 50%). **5** (Found: C, 49.62; H, 5.62; N, 8.59. $C_{27}H_{35}N_4ZnClO_7\cdot 1.5H_2O$ requires C, 49.60; H, 5.86; N, 8.58%; the presence of water in the sample sent for elemental analysis was confirmed by ^1H NMR); ν_{max}/cm^{-1}: (NH/OH) ~3370, (ClO_4) 1105, (ClO_4) 625 (KBr); δ_H (400 MHz, solvent CD_3CN): 0.96 (9H, s), 2.63 (3H, s), 2.85–3.00 (4H, m), 3.10–3.18 (2H, m), 3.88 (2H, br s), 4.58 (1H, br), 5.12 (1H, s), 6.54–6.63 (2H, m), 6.82 (1H, br s), 7.25 (5H, s), 7.40 (2H, d, $J = 7.8$ Hz), 7.60–7.65 (1H, m), 7.94 (1H, t, $J = 7.8$ Hz), 8.55 (1H, br s); δ_C (100 MHz, solvent CD_3CN): 27.7, 32.1, 32.6, 45.1, 55.1, 57.9, 63.3, 66.3, 74.4, 108.0, 112.1, 124.6, 127.2, 127.8, 128.9, 129.3, 141.9, 142.6, 149.8, 152.6, 160.4, 161.4, 179.8 (23 signals expected and observed).

X-Ray crystallography

Crystals of **1–3** were mounted on a glass fiber using a viscous oil and then transferred to a Nonius KappaCCD diffractometer with Mo-Kα radiation ($\lambda = 0.71073$ Å) for data collection at 150(1) K. For each compound, an initial set of cell constants was obtained from 10 frames of data that were collected with an oscillation range of 1 degree $frame^{-1}$ and an exposure time of 20 s $frame^{-1}$. Indexing and unit cell refinement based on all observed reflections from those 10 frames indicated a monoclinic *P* lattice for $\mathbf{1}\cdot 3CH_3CN$, a monoclinic *C* lattice for $\mathbf{2}\cdot 2CH_3CN$, and a tetragonal *P* lattice for $\mathbf{3}\cdot 0.5CH_2Cl_2\cdot 0.5CH_3CN$. Final cell constants for each complex were determined from a set of strong reflections from the actual data collection. For each data set, reflections were indexed, integrated, and corrected for Lorentz, polarization, and absorption effects using DENZO-SMN and SCALEPAC.[38] The structures of $\mathbf{1}\cdot 3CH_3CN$, $\mathbf{2}\cdot 2CH_3CN$, and $\mathbf{3}\cdot 0.5CH_2Cl_2\cdot 0.5CH_3CN$ were solved using a combination of direct methods and heavy atom using SIR 97.

For $\mathbf{1}\cdot 3CH_3CN$, the hydrogen atom on the bridging hydroxide was located and refined independently using SHELXL97.[39] All other hydrogen atoms for $\mathbf{1}\cdot 3CH_3CN$ were assigned isotropic displacement coefficients $U(H)$ (1.2 $U(C)$ or 1.5 $U(C_{methyl})$, and their coordinates were allowed to ride on their respective carbons using SHELXL97.[38] There is one disordered perchlorate anion in $\mathbf{1}\cdot 3CH_3CN$. The O(8), O(9) and O(10) oxygen atoms, bonded to Cl(2), were each split into two fragments (O(8)/O(8′), O(9)/O(9′), O(10)/O(10′)) and were refined. This refinement led to a 60 : 40 ratio in occupancy for each atom over the two positions. The hydroxyl proton of $\mathbf{1}\cdot 3CH_3CN$ participates in a weak hydrogen bonding interaction with two perchlorate oxygen atoms.

For $\mathbf{2}\cdot 2CH_3CN$ and $\mathbf{3}\cdot 0.5CH_2Cl_2\cdot 0.5CH_3CN$, the hydrogen atom on the bridging hydroxide and the secondary amine hydrogen were located and refined independently. All other hydrogen atoms were treated as riding atoms on their respective carbons as described for $\mathbf{1}\cdot 3CH_3CN$. There is one highly disordered perchlorate anion in $\mathbf{2}\cdot 2CH_3CN$. One of the two acetonitrile solvate molecules in $\mathbf{2}\cdot 2CH_3CN$ is also disordered. The C(20) and N(5) atoms were each split into two fragments (C(20)/C(20′), N(5)/N(5′)) and were refined. This refinement led to a 50:50 ratio in occupancy over each position for each atom. In the asymmetric unit of $\mathbf{3}\cdot 0.5CH_2Cl_2\cdot 0.5CH_3CN$ there are two partially occupied solvent molecules (0.25 CH_3CN, 0.25 CH_2Cl_2) disordered over the same position. The methylene chloride carbon atom (C(20)) is on a two-fold position. The chloride atom position overlaps with the position of the acetonitrile sp carbon. This overlap was modeled

as 0.5 Cl and 0.25 nitrile carbon from the respective solvents. Thus, the total chlorine count of 1.18 is an indication of this overlap. A DUMY atom was used to assist in calculating hydrogen atoms in ideal positions for the solvent.

CCDC reference numbers 282998–283000.

For crystallographic data in CIF or other electronic format see DOI: 10.1039/b512515d

Acknowledgements

This work was supported by the National Science Foundation (CAREER Award CHE-0094066). The authors thank Ewa Szajna-Fuller and Katarzyna Rudzka for assistance with experiments and manuscript preparation.

References

1 P. J. Thornalley, *Biochem. J.*, 1990, **269**, 1–11.
2 P. J. Thornalley, *Crit. Rev. Oncol. Hematol.*, 1995, **20**, 99–128.
3 P. J. Thornalley, *Chem. Biol. Interact.*, 1998, **111–112**, 137–151.
4 A. Papoulis, Y. al-Abed and R. Bucala, *Biochemistry*, 1995, **34**, 648–655.
5 A. Rahman, A. Shahabuddin and S. M. Hadi, *J. Biochem. Toxicol.*, 1990, **5**, 161–166.
6 A. D. Cameron, M. Ridderström, B. Olin and B. Mannervik, *Struct. Fold Des.*, 1999, **7**, 1067–1078.
7 S. Melino, C. Capo, B. Dragani, A. Aceto and R. Petruzzelli, *Trends. Biochem. Sci.*, 1998, **23**, 381–382.
8 C. M. Gomes, C. Frazão, A. V. Xavier, J. Legall and M. Teixeira, *Protein Sci.*, 2002, **11**, 707–712.
9 M. W. Crowder, M. K. Maiti, L. Banovic and C. A. Makaroff, *FEBS Lett.*, 1997, **418**, 351–354.
10 T. M. Zang, D. A. Hollman, P. A. Crawford, M. W. Crowder and C. A. Makaroff, *J. Biol. Chem.*, 2001, **276**, 4788–4795.
11 O. Schilling, N. Wenzel, M. Naylor, A. Vogel, M. Crowder, C. Makaroff and W. Meyer-Klauke, *Biochemistry*, 2003, **42**, 11777–11786.
12 N. F. Wenzel, A. L. Carenbauer, M. P. Pfiester, O. Schilling, W. Meyer-Klaucke, C. A. Makaroff and M. W. Crowder, *J. Biol. Inorg. Chem.*, 2004, **9**, 429–438.
13 C. Stamper, B. Bennett, T. Edwards, R. C. Holz, D. Ringe and G. Petsko, *Biochemistry*, 2001, **40**, 7035–7046.
14 A. S. Borovik, V. Papaefthymiou, L. F. Taylor, O. P. Anderson and L. Que, Jr., *J. Am. Chem. Soc.*, 1989, **111**, 6183–6195.
15 K. Matsufuji, H. Shiraishi, Y. Miyasato, T. Shiga, M. Ohba, T. Yokoyama and H. Okawa, *Bull. Chem. Soc. Jpn.*, 2005, 851–858.
16 A. W. Addison, T. N. Rao, J. Reedijk, J. van Rijn and G. C. Verschoor, *J. Chem. Soc., Dalton Trans.*, 1984, 1349–1356.
17 G. A. Russell and G. J. Mikol, *J. Am. Chem. Soc.*, 1966, **88**, 5498–5504.
18 S. S. Hall and A. Poet, *Tetrahedron Lett.*, 1970, 2867–2868.
19 L. M. Berreau, S. Mahapatra, J. A. Halfen, V. G. Young, Jr. and W. B. Tolman, *Inorg. Chem.*, 1996, **35**, 6339–6342.
20 A. L. Fuller, R. W. Watkins, A. M. Arif and L. M. Berreau, *Inorg. Chim. Acta*, DOI: 10.1016/j.ica.2005.09.008.
21 G. A. Jeffrey, *An Introduction to Hydrogen Bonding*, Oxford University Press, New York, 1997.
22 R. A. Allred, L. H. McAlexander, A. M. Arif and L. M. Berreau, *Inorg. Chem.*, 2002, **41**, 6790–6801.
23 M. Nishio, Y. Umezawa, M. Hirota and Y. Takeuchi, *Tetrahedron*, 1995, **51**, 8665–8701.
24 M. Nishio, M. Hirota and Y. Umezawa, *The CH/π Interaction: Evidence, Nature and Consequences*, Wiley-VCH, New York, 1998.
25 L. M. Berreau, R. A. Allred, M. M. Makowska-Grzyska and A. M. Arif, *Chem. Commun.*, 2000, 1423–1424.
26 D. K. Garner, R. A. Allred, K. J. Tubbs, A. M. Arif and L. M. Berreau, *Inorg. Chem.*, 2002, **41**, 3533–3541.
27 W. J. Geary, *Coord. Chem. Rev.*, 1971, **7**, 81–122.
28 R. Carballo, B. Covelo, E. Garcia-Martinez, E. M. Vazquez-Lopez and A. Castineiras, *Appl. Organomet. Chem.*, 2004, **18**, 201–202.
29 Examples of zinc hydroxide-mediated carboxy and phosphate ester hydrolysis are prevelant: (*a*) G. Parkin, *Chem. Rev.*, 2004, **104**, 699–767; (*b*) R. C. diTargiani, S. Chang, M. H. Salter, Jr., R. D. Hancock and D. P. Goldberg, *Inorg. Chem.*, 2003, **42**, 5825–5836, and references therein.
30 Reactivity of a zinc methoxide complex with thioester substrates has been reported: H. Brombacher and H. Vahrenkamp, *Inorg. Chem.*, 2004, **43**, 6050–6053.
31 C. Belle and J.-L. Pierre, *Eur. J. Inorg. Chem.*, 2003, 4137–4146.
32 X. Wang, R. Y. N. Ho, A. K. Whiting and L. Que, Jr., *J. Am. Chem. Soc.*, 1999, **121**, 9235–9236.
33 S. K. Smoukov, L. Quaroni, X. Wang, P. E. Doan, B. M. Hoffman and L. Que, Jr., *J. Am. Chem. Soc.*, 2002, **124**, 2595–2603.
34 B. Bauer-Siebenlist, F. Meyer, E. Farkas, D. Vidovic and S. Dechert, *Chem.–Eur. J.*, 2005, **11**, 4349–4360.
35 W. L. F. Armarego and D. D. Perrin, *Purification of Laboratory Chemicals*, Butterworth-Heinemann, Boston, MA, 4th edn, 1996.
36 E. Szajna, P. Dobrowolski, A. L. Fuller, A. M. Arif and L. M. Berreau, *Inorg. Chem.*, 2004, **43**, 3988–3997.
37 W. C. Wolsey, *J. Chem. Educ.*, 1973, **50**, A335–A337.
38 Z. Otwinowski and M. Minor, *Methods Enzymol.*, 1997, **276**, 307–326.
39 G. M. Sheldrick, *SHELXL-97, Program for the Refinement of Crystal Structures*, University of Göttingen, Germany, 1997.

